

Research Article

Kema terrane: A fragment of a back-arc basin of the early Cretaceous Moneron–Samarga island-arc system, East Sikhote–Alin range, Russian Far East

ALEXANDER I. MALINOVSKY,* VLADIMIR V. GOLOZOUBOV, VLADIMIR P. SIMANENKO AND
LUDMILA F. SIMANENKO

*Far Eastern Geological Institute, Far Eastern Branch, Russian Academy of Sciences, Prospect 100-letiya
Vladivostoka 159, Vladivostok 690022, Russia (email: malinovskiy@fegi.ru)*

Abstract The Kema terrane is a suite of Barremian(?)–Aptian to Albian volcano-sedimentary rocks of Sikhote–Alin that are interpreted as deposits of the back-arc basin of the Moneron–Samarga island-arc system. Compositional features of the different-type deposits indicate a near-slope depositional environment influenced by volcanic processes. Studies of slump fold orientation testify to the accumulation of material from southeast to northwest by gravitational sliding. Compositional characteristics of terrigenous rocks suggest the major provenance for detrital material was an ensialic volcanic island arc. Petrochemical characteristics of basaltic rocks indicate that the formations studied were confined to the back part of the arc.

Key words: back-arc basin, basalt, Early Cretaceous, geodynamic environment, island arc, sandstone, Sikhote–Alin, terrane, turbidite.

INTRODUCTION

The Early Cretaceous is marked by geological events responsible in many respects for the present structural pattern of the northwest Pacific continental margin. Traces of the events are recorded in terranes accreted to the Eurasian continent.

For paleogeographic reconstruction of the East Asia margin evolution in the Early Cretaceous, the studies of sedimentary basins related genetically and spatially to volcanic island arcs whose fragments have been found in Sikhote–Alin, Sakhalin and Japan are of particular value. The study of the structure, composition and depositional environments of island-arc formations can help restore their geological history as well as provide understanding of the mechanism of formation of the Sikhote–Alin folded region.

The Early Cretaceous Moneron–Samarga island-arc system has been identified by

Simanenko (1986, 1991) after summarizing vast geological and geophysical materials as well as analyzing petrochemical data of volcanic rocks. This island-arc system can be distinguished based on the occurrences of arc-related volcanoclastic formations found in some areas of the Far East region. Such formations have been found in East Sikhote–Alin (the Kema terrane) as well as on the islands of Hokkaido (Kumaneshiri Group in the Kabato Mountains) (Nagata *et al.* 1986), Rebun (Ikeda & Komatsu 1986), Moneron (Piskunov & Khvedchuk 1976) and Sakhalin (Simanenko 1986). All these formations have many common features: Early Cretaceous age, a considerable thickness, widespread occurrences of calc-alkaline volcanics, and a presence of a considerable proportion of pyroclastics in terrigenous rocks.

The Kema terrane, as a fragment of the island-arc system, has been recognized since the early 1990s (Simanenko 1991; Khanchuk *et al.* 1995). Its nature was revealed principally owing to petrochemical characteristics of the Kema volcanics

*Correspondence.

Received 29 July 2003; accepted for publication 22 February 2008.

that turned out to be similar to island-arc basalts. However, there was little evidence available to constrain the structure and composition of the sedimentary constituent of the Kema terrane. These data are needed to identify the type of basin as well as its spatial position among the Early Cretaceous structures in the Asian eastern margin.

To solve these questions, studies of the structure, composition and depositional environment of terrigenous and volcanic formations of the Kema terrane have been carried out and the studied rocks have been compared with contemporaneous rocks from the contiguous tectonic units. This paper presents the results of our research.

GEOLOGICAL SETTING

The Kema terrane is situated in the eastern portion of the Sikhote–Alin Ridge extending along the coast of the Japan Sea about 80 km in width (Fig. 1). In the Kema terrane, the Cretaceous formations are poorly exposed and available outcrops are largely restricted to the ‘windows’ in the Late Cretaceous East Sikhote–Alin volcanic belt. One such window located in the Kema River drainage area is the object of our investigation. The Kema terrane is made up of the Barremian(?)–Aptian to Albian formations, which include turbidites, debrites, volcano-sedimentary packages, as well as beds of mafic volcanics.

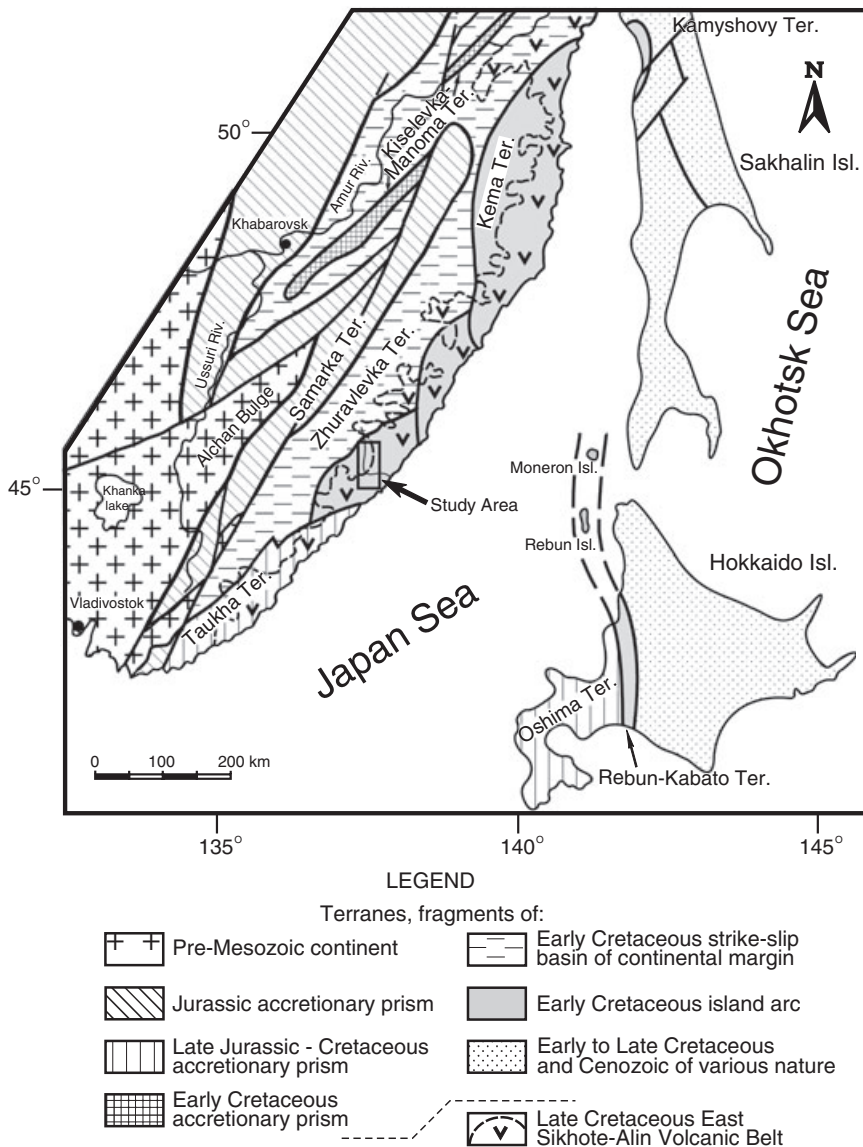


Fig. 1 Major terranes of the Russian Far East with adjacent area (after Malinovsky *et al.* 2002).

The modern tectonic structure of the Sikhote–Alin fold system represents a collage of different types of terranes, which were accreted to the East Asia margin in the Paleozoic and Mesozoic. The main part of East Sikhote–Alin is made up of Jurassic and Early Cretaceous terranes of various geodynamic natures. The following terranes are distinguished here from west to east.

The *Samarka terrane* is a fragment of the Jurassic accretionary prism that represents a tectonic package marked by an alternation of different-aged and genetically heterogeneous rocks reflecting separate episodes of the terrane formation. It consists of an arkosic matrix that contains rock fragments, blocks, and syn-sedimentary tectonic slices composed of Paleozoic–Early Mesozoic chert, sandstone, basalt, gabbroid, and limestone (Khanchuk *et al.* 1995). The analogues of the Samarka terrane are the Mino, Tamba, Ashio and some other terranes in Japan (Ichikawa 1990).

The *Taukha terrane* is a fragment of the Late Jurassic–Early Cretaceous accretionary prism. It is composed of turbidites and olistostromes with blocks and slices of Paleozoic and Early Mesozoic limestones, cherts, basalts, and terrigenous rocks (Golozoubov & Khanchuk 1995). The Taukha terrane correlates with the Early Cretaceous the Southern Chichibu terrane of southwest Japan and the Oshima terrane of Hokkaido Island (Ichikawa 1990).

The studied Kema terrane was thrust onto the adjacent unit in the west, the Early Cretaceous *Zhuravlevka terrane*. In Berriasian–Valanginian times, the Zhuravlevka terrane consisted of siltstones with rare basalt flows; the Hauterivian–Albian part of the section consists of sandstones and turbidites. The terrane is considered to be a fragment of a continental marginal strike-slip basin (Golozoubov & Khanchuk 1995).

The Early Cretaceous (Barremian through Albian) *Kiselevka–Manoma terrane* represents a package of tectonic slices that are composed of Jurassic and Early Cretaceous chert and siliceous mudstone with intercalations of basalt and limestone as well as of Early Cretaceous siltstones and turbidites (Markevich *et al.* 1997). The terrane is considered to be a fragment of the accretionary prism of the Moneron–Samarga island-arc system.

To the east of the Kema terrane lie the *Kamyshovy* and *Rebun–Kabato terranes* located on Sakhalin, Moneron, Rebun, and Hokkaido islands. Early Cretaceous geological formations composed of island arc basaltic–andesitic lavas and hyaloclas-

tics as well as of volcanoclastic sedimentary rocks are predominant in these terranes (Piskunov & Khvedchuk 1976; Ikeda & Komatsu 1986; Nagata *et al.* 1986; Simanenko 1986). The terranes are considered to be fragments of the axial part of the volcanic island arc.

OBJECTS AND METHODS OF INVESTIGATION

The Early Cretaceous volcano-sedimentary formations of the southern parts of the Kema terrane were examined in ten well-exposed sections along the Kema River and its tributaries (Fig. 2). Sedimentary structures of clastic deposits were studied in outcrops and additionally in oriented polished sections.

The petrographic composition of rocks was determined using a polarizing microscope. The modal components of sandstones were determined using standard point-counting methods, because only their fine- and medium-grained (<0.5 mm) varieties were under study. More coarse-grained sandstones composed mainly of rock fragments were not considered. Heavy minerals in sandstones were obtained by conventional crushing (≤ 0.25 mm), sieving, decanting 0.01 mm-size fractions in distilled water, and heavy liquid techniques. Mineral compositions of heavy fractions were determined and estimated by their examination through transmitted and polarized light using immersion oils. Chemical compositions of heavy minerals were determined by a JXA-5A electron microprobe. Bulk rock samples were analyzed for major elements by wet chemical analysis. Limits of detection for petrogenic oxides were 0.02–0.005%, analysis error was estimated as no more than 5%. Trace elements (Ni, Co, Cr, V, Pb, Cu, Zn, Sn) were analyzed by quantitative spectrographic analysis with an instrument sensitivity of 1–0.5 ppm. Coefficients of variation were 10–15%. Rb, Ba, Sr, Zr, Y, and Nb in most of samples was determined by X-ray fluorescence spectrometry with detection limits of 15 ppm for Ba and 2 ppm for other elements. At concentrations of more than 100 ppm the coefficient of variation is 10%.

All aforementioned analyses were performed in the laboratories of the Far Eastern Geological Institute, FEB RAS, Vladivostok. For a number of samples, large-ion lithophile and rare-earth elements as well as Hf, Ta, Th, and U were determined by ICP-MS in the analytical center of Institute of Geochemistry and Analytical

Chemistry, Siberian Branch, Russian Academy of Sciences, Irkutsk. The sample preparation for analysis and calibration of results was performed using procedures described by Rasskazov *et al.* (2003). The standard deviation for most of elements was not more than 5%. The age of palynoflora from sedimentary rocks was determined.

LITHOSTRATIGRAPHY AND AGE

The stratigraphy and sedimentological features of the Early Cretaceous successions of the Kema terrane are described briefly as follows (Fig. 2).

The lowermost part of the section consists of the Meandrovsкая Formation (>1000 m thick). It is

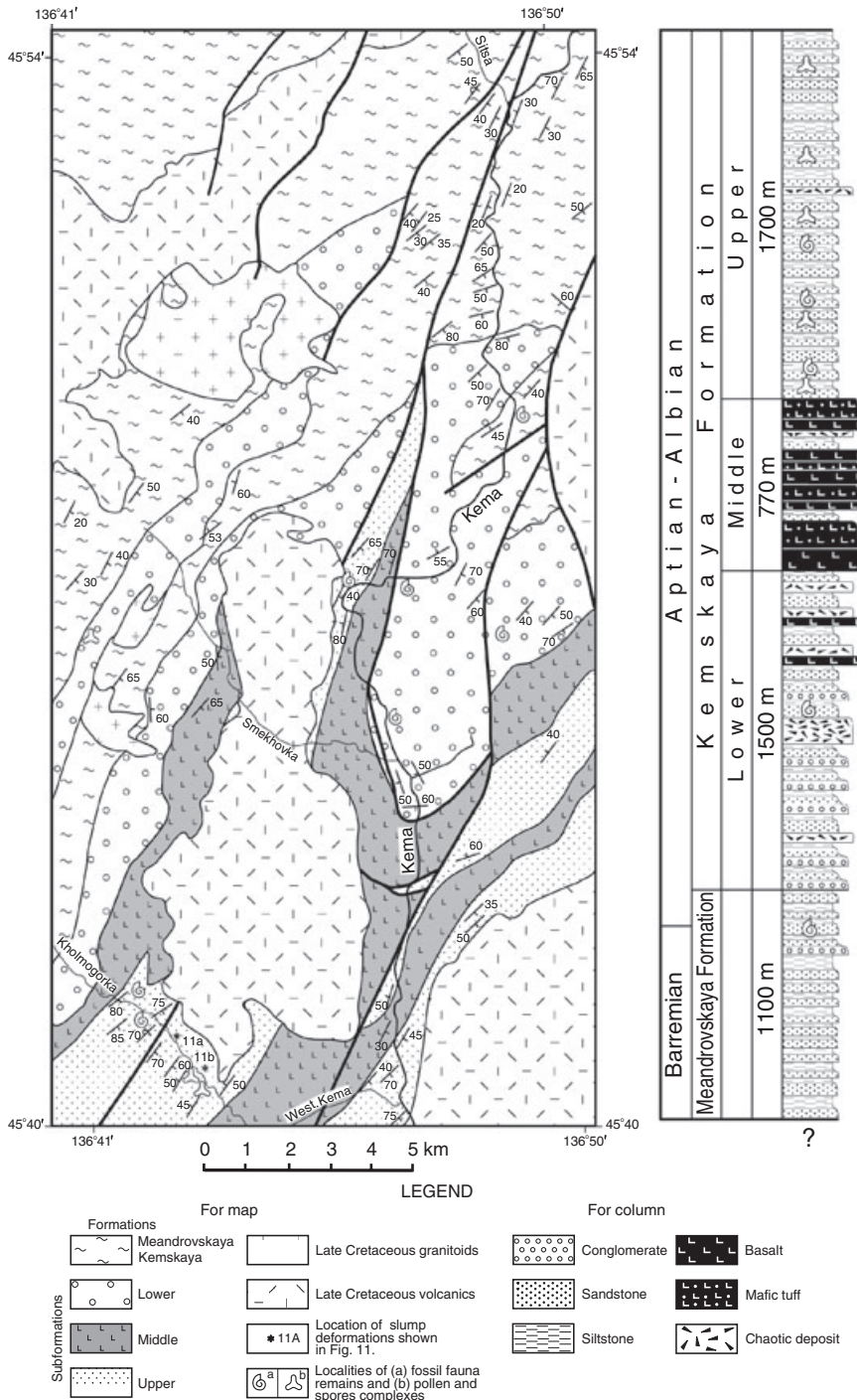


Fig. 2 Geological map and stratigraphic column showing the sequence of stratigraphic units of the Kema River Basin area.

composed of thin- to medium-bedded turbidites (3–30 cm, locally 50–100 cm). Turbidites include siltstone with thin sandstone interbeds, subaqueous slump deposits as well as massive and graded sandstone and conglomerate containing angular siltstone clasts and plant debris. Aucelline mollusks and ammonites indicate Barremian (?) to Early Aptian age for the Meandrovskaya Formation (Markevich *et al.* 2000).

The overlying Kemsкая Formation in the upper part of the succession is divided lithologically into three subformations. The *lower subformation* (>1500 m thick) consists of pebbly conglomerate (<2.5 cm), sandstone and chaotic deposits of variable composition, particle sizes and textures. Less common are turbidites, subaqueous slump deposits, tuff and solitary basalt flows with maximum thickness of 10 m. Moreover, within the subformation, the rock cycles (≤ 80 m total thickness) composed of conglomerates, sandstone, and siltstone are met. Each cycle is typified by a gradual change from pebbly conglomerate and coarse-grained sandstone to very fine-grained sandstone and clayey rock from bottom to top. The thickness of each cycle ranges from 2 to 6 m.

The *middle subformation* (770 m thick) consists of basalts, basaltic tuff and volcanoclastic sandstone. It includes rare units of rhythmically interbedded sandstone and siltstone as well as subaqueous slump deposits and debrites containing basalt blocks up to 1.5 m in size.

The *upper subformation* (≤ 1700 m thick) is made up mainly of turbiditic sequences (30–300 m thick). The thickness of the cycles ranges from 3–10 to 60–100 cm. Sandstone and siltstone are volumetrically equal parts of the cycles but locally, sandstone is predominant. The monotonous turbiditic sequence includes rare beds of siltstone, sandstone, as well as subaqueous slump deposits or may contain lump-clayey debrites.

The Kemsкая Formation is characterized by Early Aptian–Late Albian aucelline mollusks and ammonites (Markevich *et al.* 2000). Palynofloral assemblages from the lower and upper subformations are of the same age (Malinovsky *et al.* 2002).

Thus, the abovementioned features of the Barremian (?)–Aptian to Albian deposits of the Kema terrane are: (i) the large proportion of volcanic rocks in the middle part of the section; (ii) their association with coarse clastic sediments; (iii) the abundance of pyroclastics within terrigenous sequences; (iv) the predominance of turbidites in the lower and upper portions of the section; and (v)

a considerable total thickness of the deposits (≤ 5000 m) suggests high sedimentation rates.

ROCK COMPOSITION AND DEPOSITIONAL SETTING

Petrographic and geochemical characteristics of the terrigenous rocks and basaltic lavas were obtained in order to clarify the composition of the provenance and geodynamic setting of the Kema Basin.

TERRIGENOUS ROCKS

It has been recognized that the detrital composition of sandstone is significantly related to the tectonic setting of their source area. Therefore, the examination of the detrital framework modes of sandstone as well as the studies of siltstone and conglomerates provide information on the tectonic setting of the depositional basin and associated provinces (Dickinson *et al.* 1983).

Typically, all sandstones studied by modal point counts are fine- to medium-grained, moderately well sorted, and commonly angular or subrounded. Sedimentary rocks grains are more rounded than those of volcanic rocks. The matrix of the sandstone (<0.03 mm) is composed of clayey-silty material with minute grains of chlorite and volcanic glass, and it amounts to 15–40 vol.%. The fragmental portion of the rock makes up as much as 60–80 vol.% and consists of fragments of sedimentary and volcanic rocks as well as of quartz, feldspar, volcanic glass, and opaque mineral grains (Table 1). According to their modal components, the Kema sandstones have very similar compositions and are dominantly feldspathic greywacke (Pettijohn 1975).

Quartz grains are a major component of sandstone. Monocrystalline quartz is predominant and occurs as pure irregular, angular or poorly rounded, elongated grains showing undulatory extinction. Fine-grained polycrystalline quartz is much less observed. Plagioclase is the most abundant feldspar, with albite and oligoclase dominant. There are potassium feldspar grains, including somewhat altered orthoclase and minor microcline. The lithic fragments include chert, shale, and mafic and locally felsic volcanics. The fragments of metamorphic rocks are minor components. Thus, the provenance of the Kema terrane was mainly composed of sedimentary and volcanic rock assemblages.

Table 1 Average modal composition of sandstones from the Kema terrane (%)

	Meandrovskaya	Lower	Kemskaya Formation	
	Formation		Middle	Upper
	(21)	Subformation (27)	Subformation (15)	Subformation (17)
Quartz monocrystalline	31–46	33–52	31–48	36–47
	40 ± 4.1	42 ± 4.7	38 ± 4.3	41 ± 3.4
Quartz polycrystalline	2–4	3–5	2–6	3–7
	3 ± 1.1	4 ± 1.2	3 ± 1.2	4 ± 1.2
K-feldspar	1–7	1–10	2–11	1–4
	4 ± 1.9	6 ± 3.1	4 ± 2.9	3 ± 1.3
Plagioclase basic and intermediate	2–11	2–26	7–27	2–12
	6 ± 1.4	11 ± 6.4	12 ± 6.5	7 ± 3.6
Plagioclase acid	19–33	4–30	6–31	19–34
	25 ± 3.9	14 ± 8.1	19 ± 9.7	26 ± 5.1
Intermediate volcanics	4–20	3–19	14–39	4–13
	11 ± 3.8	9 ± 3.8	17 ± 6.6	6 ± 1.8
Acidic volcanics	1–6	2–5	2–7	1–5
	2 ± 1.5	3 ± 1.1	3 ± 1.7	2 ± 1.4
Metamorphic rock	0–4	0–3	0–2	0–3
	1 ± 1.2	1 ± 0.8	1 ± 0.8	1 ± 0.8
Chert	5–24	6–27	5–29	4–19
	15 ± 4.4	17 ± 4.6	13 ± 7.1	12 ± 3.9
Siltstone	4–16	3–13	3–15	4–16
	9 ± 3.2	6 ± 3.3	8 ± 4.2	9 ± 3.7

Note: At least 200 grains were counted in each sample. Content range is given in the numerator. Mean values and standard error of the mean are shown in denominator. Values in parentheses are number of samples calculated.

Paleogeodynamic interpretation of sandstone petrography was carried out by the prevalent procedures suggested by Dickinson and Suczek (1979), Dickinson *et al.* (1983), Maynard *et al.* (1982), Bhatia (1983), and Kumon *et al.* (1992). On the Qm–F–Lt diagram of Dickinson *et al.* (1983), which discriminates tectonic types of the source region, sandstone compositions plot in the field of dissected, deeply eroded, most likely epicontinental arcs (IIIa) (Fig. 3a). Sandstone compositions partially lie in the field that defines a mixed source area: remobilized orogenic belts and mature arcs (IV). The sandstones are likely derived from erosion of granitoids from the root zones of a magmatic arc and the related volcanic rocks. The tectonic settings of the Early Cretaceous sedimentary basin can be reconstructed using the diagram after Maynard *et al.* (1982). On this diagram (Fig. 3b), the sandstones studied fall simultaneously into two fields that correspond to inter-continental rifts and aulacogenes (TE) and to active continental margins complicated by strike-slip deformations along transform faults (SS). Since there is the overlap of fields on this diagram, it is impossible without supplementary data to identify unambiguously tectonic types of basin in which the sedimentation occurred. The magmatic arc type can be estimated

using the modal composition of the sandstones plotted on a diagram of the sort suggested by Kumon *et al.* (1992) (Fig. 3c). The Kema sandstones correspond to dissected and renewed magmatic arcs.

Heavy detrital minerals of the Kema sandstones are combined into two mineral assemblages. The ‘volcanic’ assemblage (~29% of the heavy minerals) is represented predominantly by typical minerals related to arc volcanics: orthopyroxene, clinopyroxene, hornblende, chromite, and magnetite. The ‘sialic’ assemblage (60% of the heavy minerals) is dominated by sialic minerals: zircon, garnet, tourmaline, epidote, apatite, sphene, and rutile.

Using the MF–GM–MT and Opx–Hb–Cpx diagrams (Fig. 4) proposed by Nechaev (Nechaev & Isphording 1993; Nechaev *et al.* 1996), the examination of heavy minerals assemblages from the Kema sandstones indicates two major provenances of detritus. When plotted in the above diagrams, most data correspond to an ensialic arc and (or) to an active continental margin with a small angle between the convergent plates, as evidenced by the low Opx concentrations. The erosion of the arc volcanics resulted in the formation of the ‘volcanic’ assemblage of the heavy detrital minerals. The provenance responsible for the supply of the ‘sialic’

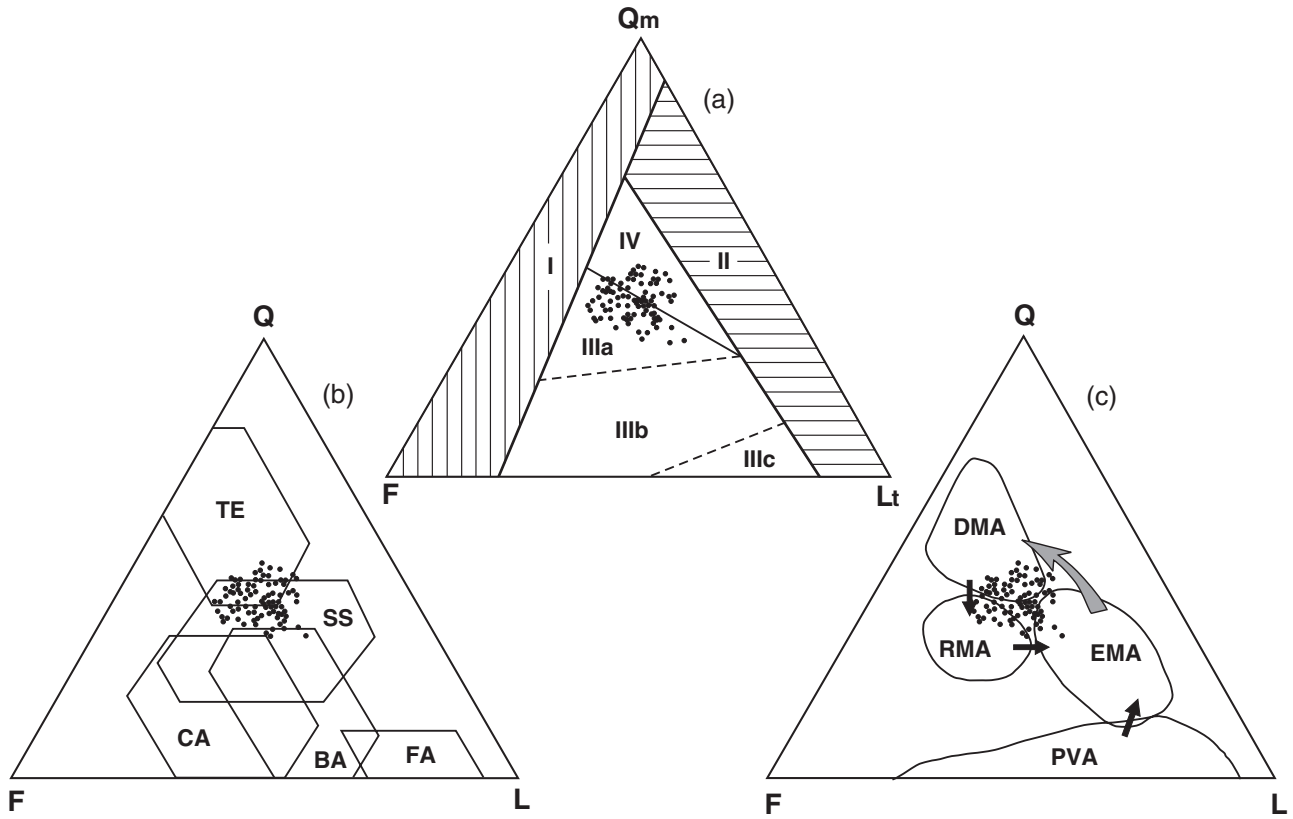


Fig. 3 Compositional diagrams of the sandstones from the Kema River Basin area and their paleogeodynamic interpretation. (a) provenance types (after Dickinson *et al.* 1983), (I, continental blocks; II, recycled orogenes; III, magmatic arc; IIIa, dissected; IIIb, transitional; IIIc, undissected; IV, mixed provenance), (b) principal types of basin environments (after Maynard *et al.* 1982). The polygons show one standard deviation about the mean. (Passive settings: TE, trailing-edge [intercontinental rifts and aulacogenes]. Active settings: CA, continental margin magmatic arcs; SS, related with strike-slip dislocations. Basins of intra-oceanic island arcs: BA, back-arc basins; FA, forearc basins), (c) discriminant diagram (after Kumon *et al.* 1992) showing magmatic arc types. Solid arrows show evolving and maturing process and gray arrow indicates unroofing and dissecting process. (Provenance types: PVA, primitive volcanic arc; EMA, evolved and mature magmatic arc; DMA, dissected magmatic arc; RMA, renewed magmatic arc. Solid circles represent sandstones from the Kema River Basin.)

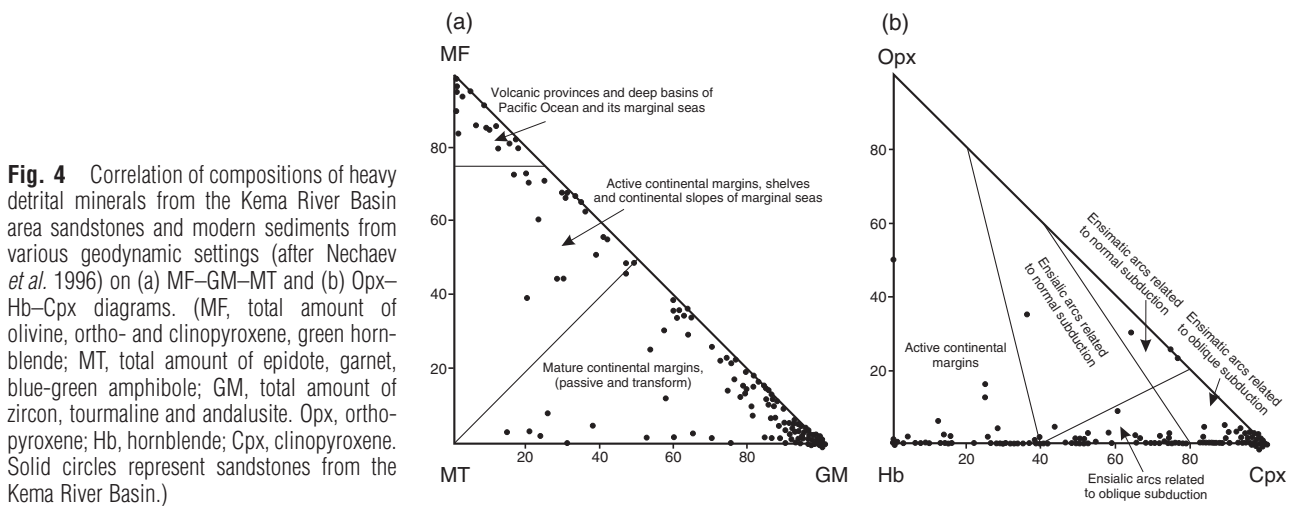


Fig. 4 Correlation of compositions of heavy detrital minerals from the Kema River Basin area sandstones and modern sediments from various geodynamic settings (after Nechaev *et al.* 1996) on (a) MF–GM–MT and (b) Opx–Hb–Cpx diagrams. (MF, total amount of olivine, ortho- and clinopyroxene, green hornblende; MT, total amount of epidote, garnet, blue-green amphibole; GM, total amount of zircon, tourmaline and andalusite. Opx, orthopyroxene; Hb, hornblende; Cpx, clinopyroxene. Solid circles represent sandstones from the Kema River Basin.)

material into the basin was probably an oceanward projection of a crustal fragment, which made up the arc basement. In this case, sedimentation in the basin could also occur due to erosion of

non-volcanic mature crust near a transform plate boundary.

The type of volcanic provenance can be further clarified through chemical composition of heavy

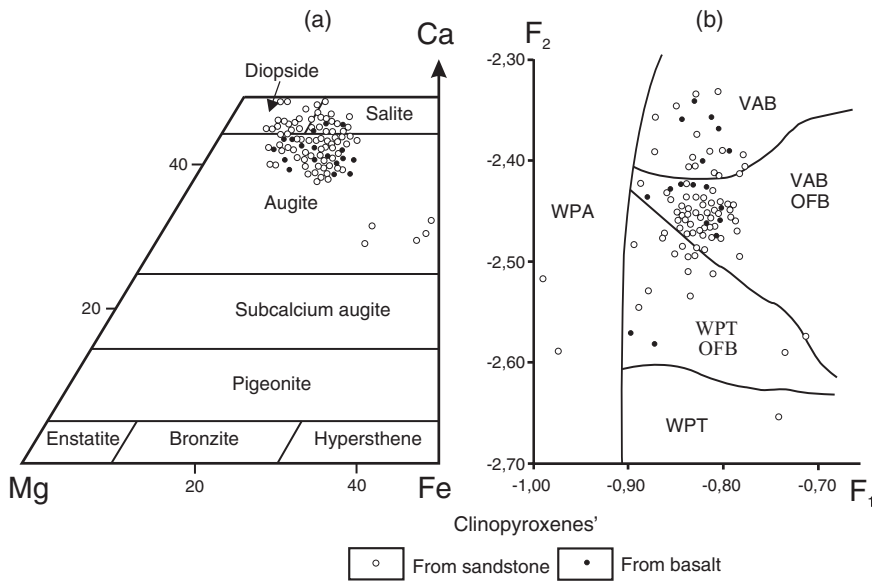


Fig. 5 (a) Diagram showing composition of detrital basalt-hosted and sandstone-hosted clinopyroxenes, and (b) discriminant diagram for basalt-hosted clinopyroxenes from different geodynamic settings (after Nisbet & Pearce 1977). (VAB, volcanic arc basalts; OFB, ocean-floor basalts; WPT, within-plate tholeiites; WPA, within-plate alkaline basalts.) $F_1 = -0.012 \times \text{SiO}_2 - 0.0807 \times \text{TiO}_2 + 0.0026 \times \text{Al}_2\text{O}_3 - 0.0012 \times \text{FeO} - 0.0026 \times \text{MnO} + 0.0087 \times \text{MgO} - 0.0128 \times \text{CaO} - 0.0419 \times \text{Na}_2\text{O}$; $F_2 = -0.0496 \times \text{SiO}_2 - 0.0818 \times \text{TiO}_2 - 0.02126 \times \text{Al}_2\text{O}_3 - 0.0041 \times \text{FeO} - 0.1435 \times \text{MnO} - 0.0029 \times \text{MgO} - 0.0085 \times \text{CaO} + 0.0160 \times \text{Na}_2\text{O}$.

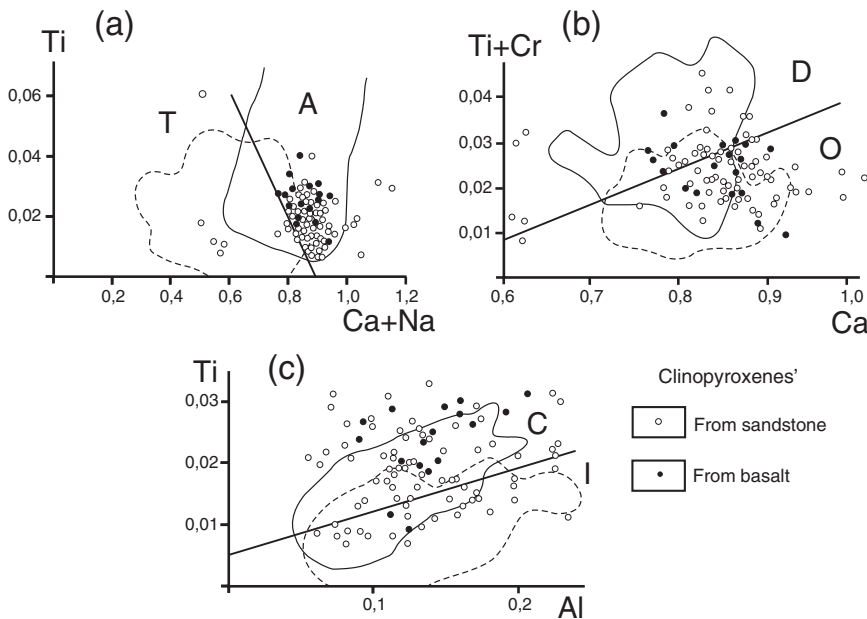


Fig. 6 Discriminant diagrams for clinopyroxenes of basalts from different geodynamic settings (after Letierrier *et al.* 1982) for (a) clinopyroxenes from alkaline within-plate (A) and non-alkaline (T) basalts, (b) clinopyroxenes of non-alkaline basalts distinguishing MORB (D) from calc-alkaline and tholeiitic basalts of epycontinental and island arcs (O), and (c) clinopyroxenes from calc-alkaline (C) and tholeiites of epicontinental and island arcs (I). Fields corresponding to the composition of clinopyroxenes from different basalts are represented by solid and dashed lines. Elements are given in formula units.

minerals. The diagrams for clinopyroxene composition (Figs 5,6) illustrate a correlation between the clinopyroxenes from sandstones of the Kemsкая and Meandrovskaya Formations and those from basaltic rocks in the Kemsкая Formation. Compositions of clinopyroxenes from sandstones plot in the same region and are compositionally similar to clinopyroxenes from basalts. On the ternary Mg–Ca–Fe diagram (Fig. 5a), all clinopyroxenes fall into fields that correspond to augite, diopside, and salite. According to the discriminant diagram after Nisbet and Pearce (1977) (Fig. 5b), most of the Kema clinopyroxenes fall into fields that correspond to volcanic arc basalts, with the

remainder representing ocean floor basalts. The discriminant diagrams of Ti vs Ca+Na, Ti+Cr vs Ca and Ti vs Al in Figure 6 (Letierrier *et al.* 1982) discern the difference between basalt-hosted pyroxenes from various geodynamic settings. On the Figure 6a, clinopyroxene compositions (including basalt-hosted ones) are situated near the line separating clinopyroxenes of alkaline (A) within plate (island-arc and intracontinental) basalts and of all other non-alkaline basalts (T). Formally, the clinopyroxenes may be assigned to alkaline basalts, but rather low Ti and Na contents do not make it possible to attribute these clinopyroxenes to this basalt type. On Figure 6b, considering the non-

alkaline basalts as MOR (mid-ocean ridge) basalts (D) and tholeiitic and calc-alkaline basalts of continental-margin and island arcs (O), the clinopyroxenes studied either lie within the area of the island-arc basalts or occur immediately adjacent to this area. Figure 6c, subdividing the island-arc clinopyroxenes into calc-alkaline (C) and tholeiitic (I) clinopyroxenes, demonstrates that our pyroxenes were derived from calc-alkaline basalts typical of the back-arc zone of island arcs. As indicated in Figure 7 (after Arai 1992), showing the composition of detrital chrome spinels from the Kema sandstones, many of the data for this mineral fall into the field of island-arc basalts and a portion of those correspond to the area of high-alkaline within-plate basalts and mid-oceanic ridge basalts (MORB) that could be part of the accretionary prism partaking in the arc basement. The composition of amphiboles, which were found in the same heavy fraction and are essentially identical to those expected for volcanics from island arcs, imply that island-arc rocks constituted the principal source for these detrital minerals.

The chemical compositions of the Kema River basin sandstones are: SiO₂, 65–83; TiO₂, 0.12–0.66; Al₂O₃, 6.30–13.92; FeO + Fe₂O₃, 0.98–5.52; MgO, 0.20–3.12; Na₂O, 1.06–2.80; and K₂O, 0.94–3.50 wt.%. A genetic interpretation of the chemical composition of the sandstones is presented on the discriminant diagrams (Fig. 8). On the diagram after Bhatia (1983) (Fig. 8a) used for discrimination of sandstones from the basins attributed to different geotectonic settings, the majority of the exam-

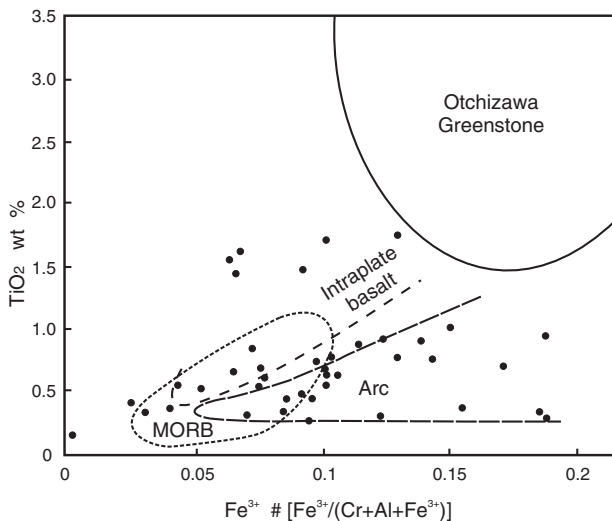


Fig. 7 Chemical characteristics of detrital chrome spinels from Kema sandstones (solid circles). Discrimination lines for magma chemistry (after Arai 1992) are shown.

ined sandstones can be grouped into the fields suggesting the basins of active continental margin and the basins connected with arcs developed on the mature continental crust. The low Mg and total Fe contents in the sandstones keep their figurative points partially away from the field of epicontinental island arcs. This can be accounted for by high 'maturity' of rocks related to their enrichment in silica. On the diagram after Maynard *et al.* (1982) (Fig. 8b), the sandstones studied show considerable scattering but with some affinity to sandstones typical of the basins related to passive continental margin and with sandstones related to continental margin arcs. The deviation of the data of sandstones on the K₂O/Na₂O–Fe₂O₃* + MgO and SiO₂/Al₂O₃–K₂O/Na₂O diagrams from the fields corresponding to basins of continental margin magmatic arcs can be due to abundant fragments of K-rich basalt (shoshonite).

Chemical compositions of siltstones and associated sandstones are similar. Thus, the paleotectonic interpretation of the siltstone chemical composition (Fig. 8c) is consistent with the interpretation obtained from the sandstones but shows less variability.

Conglomerates at various stratigraphic levels of the examined section comprise chert clasts with Triassic and Jurassic radiolarians. Thus, the Jurassic to Early Cretaceous accretionary prism (similar to the accretionary prisms of the Samarka and Taukha terranes of the Sikhote–Alin region) can be considered as a constituent part of the volcanic island arc basement (Khanchuk *et al.* 1995; Malinovsky *et al.* 2002).

VOLCANIC ROCKS

The volcanic part of the section studied is represented by basalt, hyaloclastite, as well as by their tuffs ranging widely in size and sorting of their constituent particles, which may contain separate beds of turbidites, sandstones, and debrites. Commonly, the basalts display pillow structure with pillows ranging in size from 0.5 to 2.5 m. The basal parts of lava flows are abundant in inclusions of sediments. The upper levels are represented by massive lava. The thick layers of the lava flows contain 'floating' inclusions (i.e. not in contact with each other) of flattened blocks of sedimentary rocks oriented parallel to the direction of lava movement. The thin lava layers (up to 1 m) were cracked and split into segments. The vertical fractures between these segments were filled with siltstone that at the time of lava eruption was unconsolidated silty

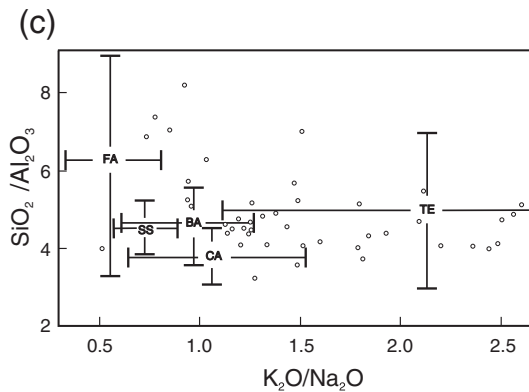
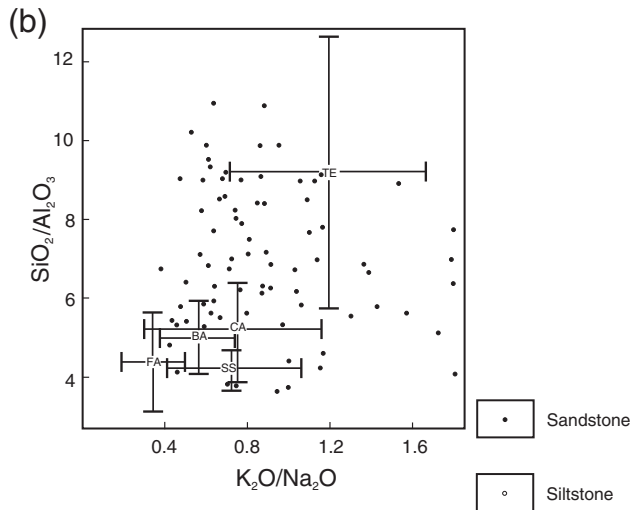
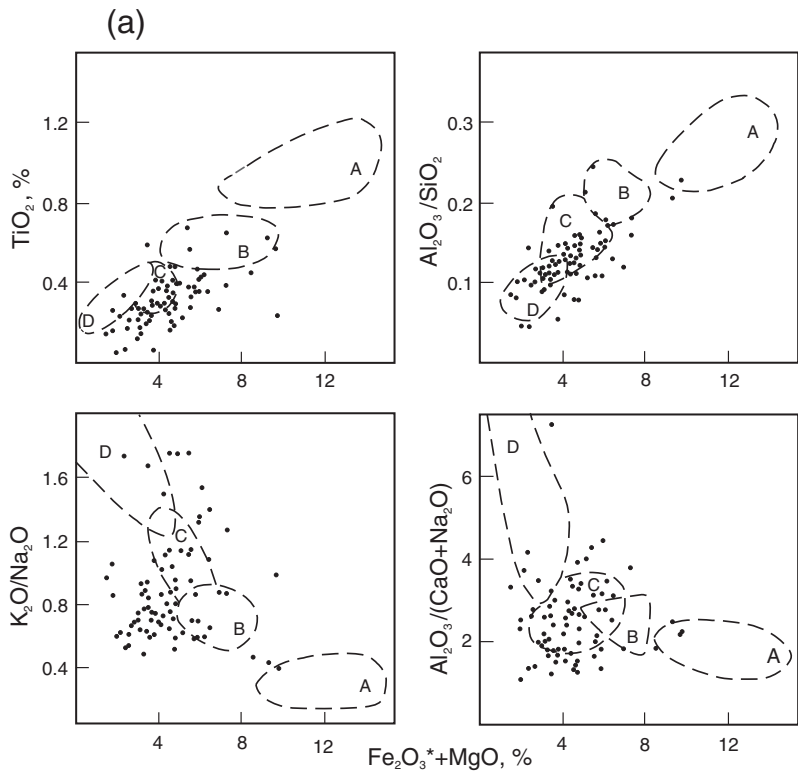


Fig. 8 Diagrams representing chemical compositions of sandstones and siltstones from different geodynamic settings. (a) Basin types, according to Bhatia (1983). Dotted lines are field boundaries for the geochemical parameter values of the ancient sandstones from basins related to A, oceanic island arcs; B, continental island arcs; C, active continental margins; and D, passive continental margins. $Fe_2O_3^*$ = all iron as Fe_2O_3 . (b) and (c) basin environments, according to Maynard *et al.* (1982). (b) for sandstones, (c) for siltstones. Crossed lines indicate standard deviation from the average compositions of modern deep-sea sandstones and clays. See Figure 3 for explanation of the abbreviations.

sediment. Under basalt mass loading this soft sediment was squeezed up along fractures forming 'sedimentary dykes'. Sometimes the soft silty material came out onto the lava surface. Basaltic 'drops' or bombs with glassy or zeolite fringes can be observed within the siltstone.

The pyroclastic material accounts for approximately 20% of total thickness of the *middle sub-formation* of the Kemska Formation. It is represented by basalt tuff. Tuffs commonly show graded bedding. The base of tuff layers is made up of agglomerate tuff. Toward the roof tuff layers become more fine-grained. The upper units are represented by psammitic and pelitic tuffs.

The basalts are fully crystalline. Mafic mineral and plagioclase phenocrysts up to 8 mm across may constitute 10–35% of the rock volume. Amid pillow lavas, amygdaloidal basalts with amygdaloids of 1–5 mm composed of chlorite, calcite, and scarce zeolite are present. The matrix textures are dominantly tholeiitic, vitrophyric, intersertal, and microlitic. Diabasic texture is less common. According to phenocryst type and its modal percentage in the rock, the basalts studied are subdivided into clinopyroxene–plagioclase, olivine–clinopyroxene–plagioclase, olivine–clinopyroxene, and two-pyroxene types. If we take the total amount of phenocrysts as 100%, the clinopyroxene–plagioclase basalts contain 50–65% plagioclase phenocrysts, 35–50% clinopyroxene phenocrysts and rare phenocrysts of olivine and brownish-green hornblende. In olivine–clinopyroxene–plagioclase basalts, olivine content increases up to 1–2%. The olivine–clinopyroxene basalts have 5–7% olivine phenocrysts, 10–20% plagioclase phenocrysts, and 60–65% clinopyroxene phenocrysts. The two-pyroxene basalts, together with the rest minerals, contain up to 5% orthopyroxene phenocrysts.

The core parts of clinopyroxene phenocrysts in olivine–clinopyroxene basalts are composed of diopside or salite (Fig. 5a) and its rims correspond to augite. In other basalt varieties, clinopyroxene is represented predominantly by augite. The cores of the clinopyroxene phenocrysts have Mg# 89–84 and edge parts of these phenocrysts show lower Mg# (75–72). Clinopyroxenes are replaced with amphiboles of the tremolite–actinolite series, chlorite with some amounts of dusty opaque minerals, and carbonates. Olivine and orthopyroxene are almost entirely replaced with secondary minerals: chlorite–serpentine–prehnite aggregates, carbonate, talc, and brown-colored lepto-chlorite. Plagioclases occur as euhedral phenocrysts and glomerocrysts with olivine and clinopyroxene. A

number of plagioclase phenocrysts contain residual volcanic glass inclusions. Plagioclase compositions range from An_{75–86} in central parts of the phenocrysts to An₅₀ in its edge parts. The chemical composition of a residual glass inclusions in plagioclase is: SiO₂, 61.92; TiO₂, 0.62; Al₂O₃, 18.58; Cr₂O₃, 0.40; FeO, 1.92; MnO, 0.07; MgO, 0.50; CaO, 1.60; Na₂O, 1.66; and K₂O, 9.98 wt%.

A groundmass of the basalts consists of plagioclase, orthoclase, clinopyroxene microlites, magnetite, and volcanic glass. Flakes of biotite are sparsely distributed in mesostasis of olivine–clinopyroxene basalts. The characteristic features of minerals making up mesostasis are as follows. Clinopyroxenes show low Mg# (62). Plagioclase microlites compositions range from An₄₅ to An₅₀ and are similar to marginal zones of plagioclase phenocrysts. According to the silica content (SiO₂ = 56.4–56.9%), volcanic glass is close to andesite. It exhibits a high content of aluminum oxide (Al₂O₃ = 17.6–20.8%) and high alkalinity (K₂O = 2.4–3.1%, Na₂O = 3.8–4.5%). Volcanic glass in mesostasis is replaced with chlorite and carbonates with local zeolites and analcite.

Chemical analyses of major petrographic varieties of the basalts are presented in Table 2. The rocks have low SiO₂ and TiO₂ contents (44–50 and 0.7–1.25%, respectively), moderate MgO contents (3.9–8.9%), and high Al₂O₃ and K₂O contents (15.1–19.1 and 1.6–3.9%, respectively). From the data on SiO₂ vs alkalinity ratios (Peccerillo & Taylor 1976), the basalts belong to high-K calc-alkaline and sub alkaline series. The olivine–clinopyroxene and two-pyroxene basalts correspond to absarokite, but olivine–clinopyroxene–plagioclase and clinopyroxene–plagioclase basalts correspond either to shoshonitic basalts with lower MgO contents (<5%) or to high-potassium basalts. FeO*/MgO (FeO* = all iron as FeO) ratios in absarokites are 0.86–1.48 increasing up to 1.6–1.9 in clinopyroxene–plagioclase basalts.

Basalts are characterized by the low contents of iron-group elements (Sc, V, Cr, Co, Ni) (Table 2). Iron-group elements compatible with crystallizing olivine and pyroxene as well as a number of incompatible elements (Ti, Zr, Hf, Ta, REE, Th, U) show good correlations with MgO and FeO*, which can evidence the stability of these elements during postmagmatic processes. This makes it possible to use them in geodynamic interpretations (Simanenkov *et al.* 2004). Contents of large-ion lithophile elements (LILE) are in general elevated, which are typical of basalts of calc-alkaline and shoshonite series in different regions.

Table 2 Major (wt%) and trace element (ppm) analyses for the Kema Formation basalts

Sample no. Locality no.	1 KM-503	2 KM-507	3 KM-509	4 KM-511	5 KM-516	6 KM-519	7 KM-514	8 KM-520
SiO ₂	46.40	44.80	48.80	49.30	48.80	50.66	48.40	46.00
TiO ₂	0.93	1.10	0.78	0.75	0.99	0.80	0.83	0.84
Al ₂ O ₃	15.10	15.60	15.70	15.80	18.50	17.80	17.70	18.30
Fe ₂ O ₃	2.05	3.50	2.51	1.94	4.83	3.10	3.90	4.70
FeO	5.74	5.37	6.38	7.52	4.20	4.20	3.60	3.30
MnO	0.15	0.15	0.15	0.16	0.12	0.12	0.13	0.18
MgO	8.85	6.92	5.80	5.83	4.60	4.70	5.47	5.30
CaO	8.42	11.00	9.02	9.66	8.80	8.80	12.40	12.50
Na ₂ O	2.80	1.80	4.30	2.40	3.50	2.80	2.50	2.20
K ₂ O	1.50	2.00	1.45	1.85	1.64	2.30	1.70	1.60
P ₂ O ₅	0.32	0.39	0.31	0.28	0.33	0.26	0.35	0.30
H ₂ O ⁻	0.21	1.36	0.34	0.45	0.28	0.03	0.31	0.42
LOI	7.11	5.65	4.00	4.02	3.10	4.00	3.06	3.95
Total	99.58	99.64	99.84	99.96	99.69	99.51	100.35	99.49
Sc	49.1	24.8	53.4	35.1	25.2	27.6	35.7	26.2
V	150	170	200	240	230	220	300	260
Cr	170	210	80	91	20	100	145	62
Co	24	34	27	29	18	16	37	23
Ni	130	150	50	54	29	73	81	62
Cu	118	55.6	135	45.4	83.6	50.2	110	97.4
Zn	131	63.2	103	53.4	55.6	41.2	50.8	56.1
Ga	8	12	12	13	10	11	16	12
Rb	60.7	59.7	49.4	44	31.2	86	33.4	16.7
Sr	997	575	581	532	588	491	749	567
Y	30.9	20	33.6	19.2	24.7	17.8	20.4	21.2
Zr	102	88.6	106	49	74.3	55.4	47.8	47.8
Nb	10.8	45.1	6.91	3.66	5.0	5.64	4.44	3.39
Mo	1.6	2.5	–	–	–	1.5	1.6	–
Ag	1.6	0.11	10	0.32	0.46	0.60	0.10	0.20
Sn	4	3	2	3	3	2	2	1
Ba	2121	657	268	162	122	334	122	266
Hf	2.94	2.32	3.38	1.31	2.08	1.34	1.25	1.53
Ta	0.61	2.86	0.48	0.32	0.46	0.29	0.32	0.32
W	0.25	0.07	0.55	0.05	0.03	0.17	0.07	0.09
Pb	32.1	9.6	18.9	1.02	1.96	1.52	1.21	2.42
Th	6.88	4.39	12.0	2.04	2.15	2.10	1.94	2.53
U	1.72	1.10	2.56	0.54	0.78	0.71	0.67	0.77
La	22.4	26.3	24.1	10.9	12.8	12.1	13.1	12.0
Ce	51.8	47.3	59.0	23.3	27.9	24.7	27.3	25.4
Pr	6.96	5.23	7.29	3.11	3.73	3.09	3.55	3.33
Nd	29.1	22.4	33.7	15.6	18.2	14.8	17.4	16.1
Sm	6.83	4.25	7.24	3.43	3.93	3.17	3.58	3.63
Eu	2.20	1.31	2.16	1.02	1.24	0.99	1.15	1.17
Gd	7.53	4.15	7.44	3.61	4.38	3.30	3.83	3.89
Tb	1.02	0.63	1.13	0.54	0.67	0.49	0.56	0.59
Dy	5.57	3.45	5.83	3.25	3.97	2.23	3.32	3.45
Ho	1.21	0.69	1.32	0.66	0.88	0.61	0.69	0.72
Er	3.17	1.90	3.77	1.89	2.45	1.72	2.02	2.05
Tm	0.57	0.31	0.64	0.31	0.42	0.29	0.34	0.32
Yb	3.45	1.99	4.23	1.92	2.64	1.87	2.19	2.13
Lu	0.52	0.29	0.57	0.29	0.42	0.31	0.34	0.32

Note: 1–3, olivine-clinopyroxene basalts (Ol_{5–7}, Cpx_{75–80}, Pl_{10–20}); 4–6, two-pyroxene basalts (Ol_{5–7}, Opx₅, Cpx_{60–70}, Pl_{15–20}); 7–11, olivine-clinopyroxene-plagioclase basalts (Ol_{1–2}, Cpx_{60–70}, Pl_{28–30}); 12–15, clinopyroxene-plagioclase basalts (Cpx_{35–50}, Pl_{50–65}, Amf ±). LOI, loss on ignition; –, not detected.

9 KM-536	10 KM-538	11 KM-563/3	12 KM-512	13 KM-515	14 KM-517	15 KM-517/1
48.30	48.90	47.00	49.50	48.6	49.10	49.5
0.70	0.80	1.20	0.82	0.80	0.73	0.70
19.70	18.50	19.40	17.50	18.80	16.40	15.50
3.80	1.80	3.40	1.89	4.70	4.60	4.20
4.20	6.10	3.60	6.80	2.90	3.06	3.20
0.12	0.13	0.08	0.13	0.11	0.18	0.17
4.80	5.10	3.60	4.81	3.90	4.70	4.20
10.10	9.10	10.40	6.70	11.10	9.10	11.40
2.50	2.70	2.80	2.80	3.12	3.50	2.60
2.60	3.50	2.40	3.94	2.05	2.60	1.60
0.40	0.28	0.33	0.34	0.28	0.42	0.26
0.10	0.14	0.27	0.23	0.6	0.38	0.92
2.80	2.60	5.30	4.00	2.60	5.44	5.42
100.12	99.61	99.79	99.46	99.56	100.21	99.67
26.2	31.3	26.5	27.6	25.9	28.0	25.2
290	230	170	230	260	260	180
34	83	59	63	50	43	88
21	24	18	19	23	15	23
45	58	49	44	55	33	62
99.0	85.2	31.8	61.8	91.7	76.4	45
31.2	43.3	47.4	55.9	47.7	41.6	41.1
12	16	11	16	15	11	12
66.5	89.3	53.5	142	29.8	93.8	25.7
594	486	449	753	525	410	351
17.9	20.2	17.6	21.5	21.6	19.8	19.0
47.8	44.1	60.8	59.1	70.0	49.3	51.6
3.49	5.37	7.64	4.65	4.46	3.13	2.57
–	–	1.5	–	–	–	1.5
0.46	0.16	1.20	0.59	0.20	0.25	0.20
3	2	3	2	2	2	3
329	455	355	335	146	285	232
1.32	1.36	1.44	1.60	1.77	1.24	1.24
0.26	0.49	0.65	0.37	0.38	0.23	0.21
0.14	0.33	0.09	0.12	0.07	0.18	0.08
0.67	2.58	2.66	1.54	1.98	2.68	5.82
2.53	2.71	2.32	3.01	2.84	2.55	4.06
0.98	0.92	0.59	0.95	0.85	1.02	0.98
12.2	12.1	12.1	15.1	12.7	10.2	13.1
26.8	26.3	26.0	31.5	28.0	21.8	26.9
3.56	3.43	3.15	4.13	3.60	2.89	3.29
17.9	17.1	15.3	19.0	16.8	14.6	15.1
3.80	3.77	3.46	4.00	3.48	3.30	3.35
1.08	1.08	1.22	1.11	1.12	1.01	0.96
3.68	4.00	3.64	3.95	3.77	3.52	3.51
0.54	0.59	0.55	0.61	0.58	0.56	0.54
3.14	3.41	3.06	3.46	3.49	3.25	3.15
0.64	0.70	0.64	0.74	0.73	0.68	0.67
1.94	2.03	1.77	2.11	2.16	2.06	1.91
0.29	0.33	0.28	0.33	0.36	0.34	0.31
1.88	2.120	1.72	2.19	2.32	2.16	1.98
0.29	0.33	0.26	0.33	0.36	0.33	0.31

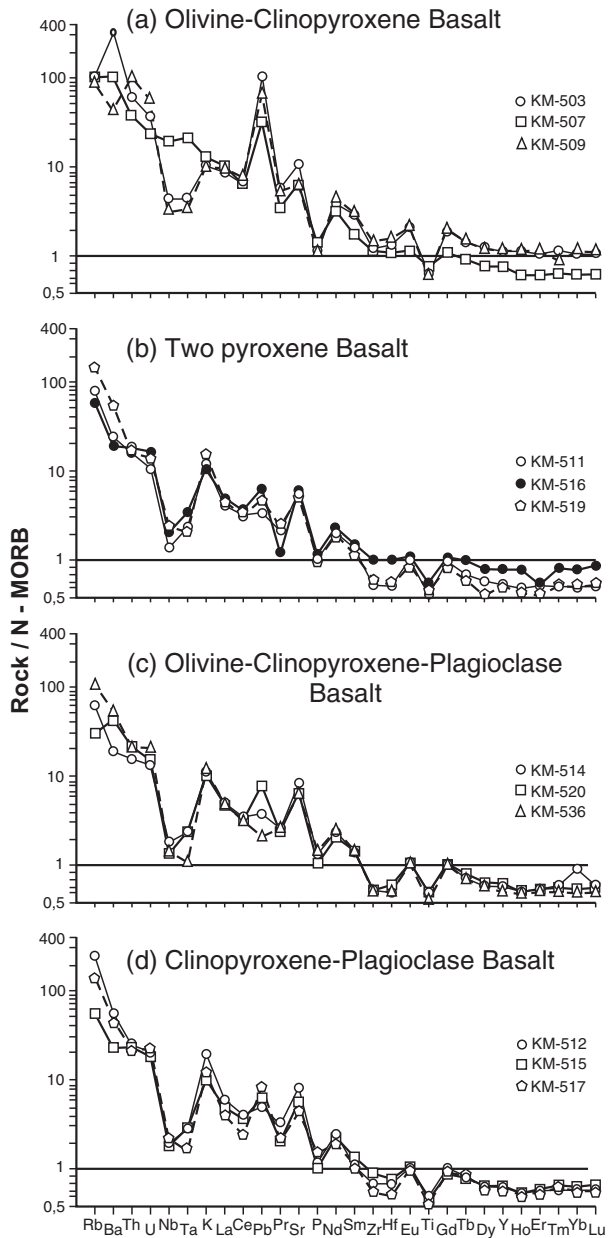


Fig. 9 Incompatible trace element abundances normalized to N-MORB values (after Sun & McDonough 1989). Locality numbers shown are explained in Table 2.

Spider diagrams (Fig. 9) for basalts clearly illustrate the similarities and differences in their trace element compositions (Table 2), which have been normalized to N-type MORB (Sun & McDonough 1989). It is evident from the diagrams that the Kema basalts are enriched in LILE relative to N-type MORB and depleted in high fusible elements (HFSE) and in heavy rare earth elements (HREE) relative to N-MORB basalts. All rock varieties are characterized by positive Rb, Ba, Th, U, K, Pb, and Sr anomalies and by negative Ta, Nb, P, Zr, Hf, and Ti anomalies. Compared to other

petrographic varieties of basalts, the olivine-clinopyroxene basalts (absarokites) are richest in LILE, HFSE, and HREE. In contrast, the compositions of the entire Kema basaltic series are consistent with derivation from the most primitive absarokitic magma by differentiation by ferromagnesian mineral (olivine and pyroxene) fractionation indicating a suprasubduction nature of the magma. Other diagrams (Rollinson 1994) are presented in Figure 10 and the values of trace element indicator ratios demonstrate that the Kema basalts have an affinity with island-arc-type magmas. However, on the diagrams TiO_2 vs FeO^*/MgO and V vs Ti (Fig. 10b,c), trace element ratio data for some basalts are somewhat shifted to the area of back-arc basin basalts. Therefore, it can be expected that the formation of the Kema volcanites occurred in the rear zone of the island arc adjacent to the back-arc basin.

DISCUSSION

DEPOSITIONAL ENVIRONMENTS OF THE KEMA TERRANE FORMATION

The Meandrovszkaya and Kemszkaya Formations are characterized by an abundance of geological units with cyclic intercalations of sandstone and siltstone beds. The cycles forming these units show erosive bases with rip-up clasts from the underlying deposits, a set of sedimentary structures with the following patterns of the Bouma sequence: abcde, bde, bcde, and cde. All these signatures are typical of turbidites (Walker 1978). Turbidites are commonly associated with slump and chaotic beds, pebbly conglomerates, sandstones, and siltstones, which show the gradual change of lithofacies. The clastic sediments were deposited by gravity flows. Siltstones with thin sandstone interlayers that were probably deposited by floor currents are volumetrically minor. The composition of the deposits suggests that they formed at the base of submarine slopes as well as in the adjacent areas of the basin plain.

The position of basalts within the volcano-sedimentary sequence, their fabric features as well as their association with turbidites and subaqueous slump formations suggest that they were formed by submarine volcanic eruptions. Lavas erupted onto unconsolidated sediments in a submarine environment. Relatively good sorting of tuff and the coarse nature of its constituents suggest an explosive style of eruption, deposition of pyroclastic fragments from eruption clouds, differentiation and

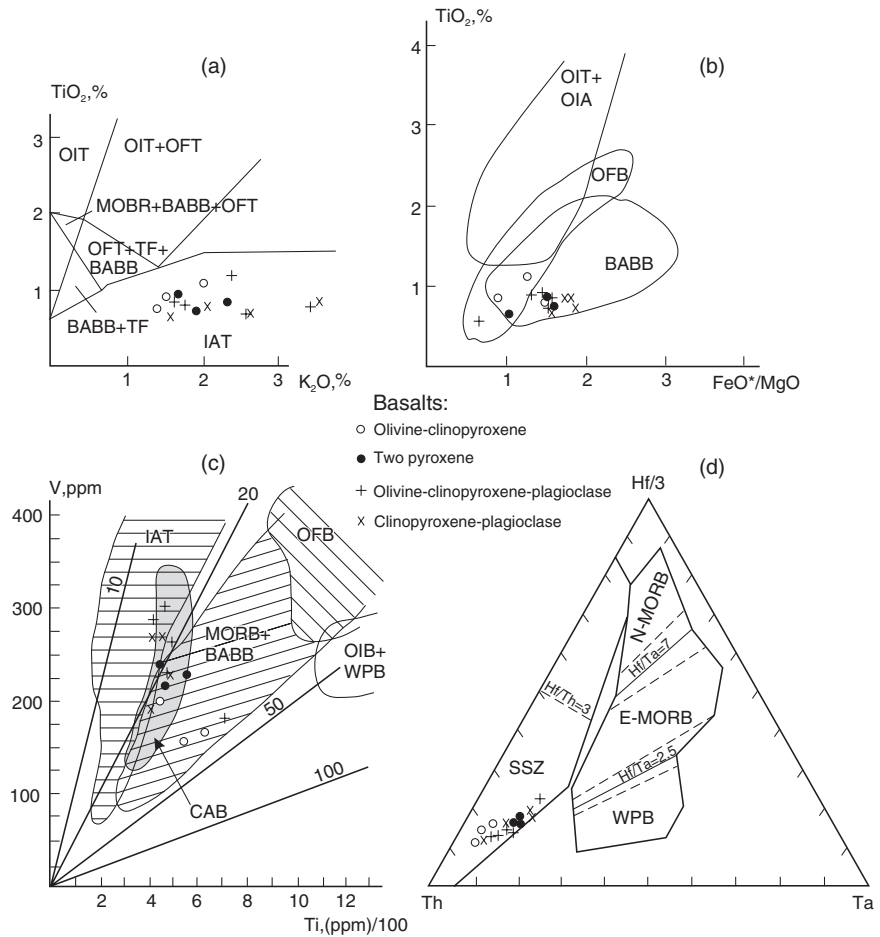


Fig. 10 Variation diagrams showing (a) TiO_2 vs K_2O (after Mironov 1990), (b) TiO_2 vs FeO^*/MgO (after Kimura *et al.* 1994), and (c) $V-Ti$ (after Shervais 1982); and (d) discriminant diagram for $Hf/3-Th-Ta$ (after Wood 1980). BABB, back-arc basin basalts; MORB, mid-ocean ridge basalts [N-MORB, normal MORB; E-MORB, enriched MORB]; OFB, ocean-floor basalts; OIT, ocean island tholeiites; OFT, ocean-floor tholeiites; OIA, ocean island alkaline basalts; OIB, ocean island basalts; WPB, within-plate basalts; IAT, island arc tholeiites; CAB, calc-alkaline basalts; SSZ, suprasubduction zone basalts; TF, transform fault.

reworking of volcanic material in an aqueous environment, as well as indicating that the deposition of tuffs occurred in close proximity to volcanic edifices. The above data on the mineralogy and chemistry of terrigenous rocks are indicative of their significant influence on the formation of a turbidite sequence. The geochemical characteristics of the studied basalts showing the subalkaline (shoshonitic) and K-rich calc-alkaline affinities indicate that volcanic deposits formed within the back zone of the island arc during the final stages of its formation (Simanenko 1991).

Thus, it is possible to assume that accumulation of the Kema terrigenous deposits occurred in a near-slope environment influenced by volcanic processes. The major transportation agents for the conveyance of clastic material were sediment gravity flows of various types. To ascertain a flow direction, slump folds in turbidites at different stratigraphic levels of the Meandrovskaya Formation and the upper Kemskaya subformation have been studied by Malinovsky *et al.* (2002). In the Kholmogorka Creek Basin area in the northwestern limb of the syncline (Fig. 2), slumping struc-

tures are exposed (Fig. 11a). The relatively more lithified sandstone beds above mudstone-dominant interbeds have been deformed into a set of overturned microfolds. In the southeastern limb of the same syncline, a horizon containing slump folds was observed at approximately the same stratigraphic level (Fig. 11b). In all observed cases (>50 observations), the hinge lines of the examined folds are nearly horizontal (Fig. 11c), so that a trend of a submarine slope, on which the sediments accumulation occurred, agrees with the syncline trend of a northeast direction (35–45°). The vergence of slump folds in both limbs of the syncline indicates northwesterly gravitational sliding of the material. To reconstruct the paleoslope orientation, the original trends of the sublatitudinal Sikhote–Alin fold structures should be considered (70–80°) (Utkin 1980). The present northeast–southwest direction of strata is interpreted as the result of counter-clockwise rotation during the later displacements along the system of the continental marginal north–northeast-trending sinistral strike slip faults. Thus, the clastic material was supplied not from the northwest, but from

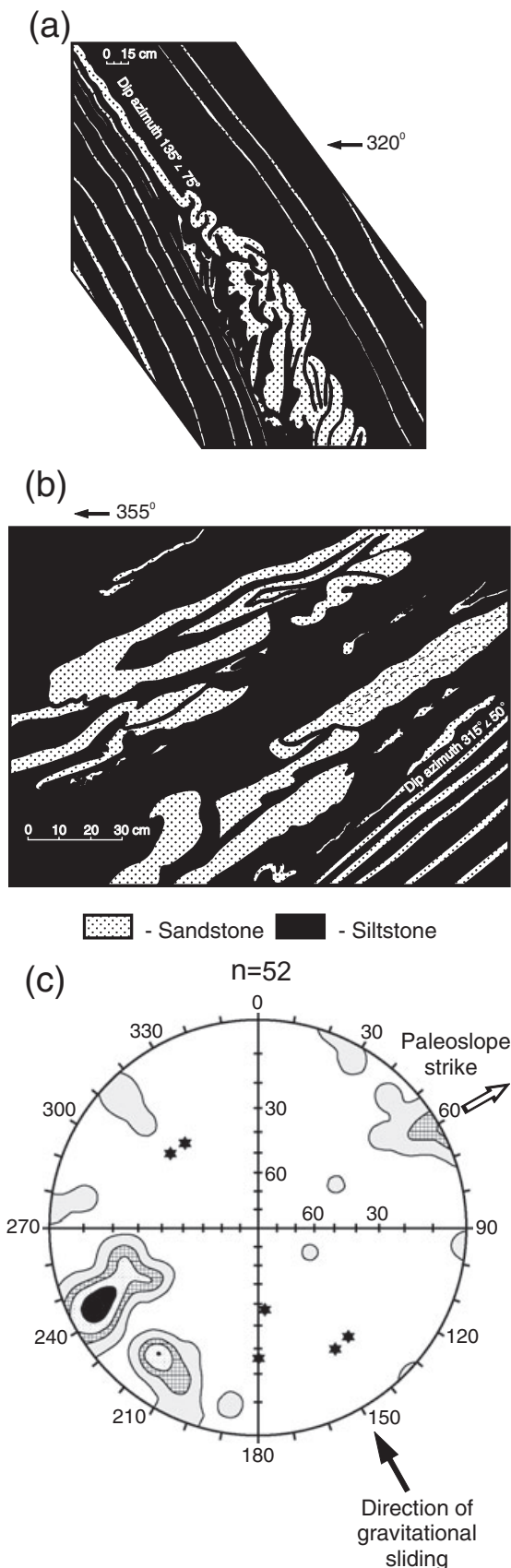


Fig. 11 (a, b) Outcrop sketches of slump deformations observed in the upper subformation of the Kemsкая Formation (left bank of the Kholmogorka Creek). Locations of outcrops are shown in Fig. 2. (c) Diagram of the position of slump fold hinges in the Kema River Basin. Wulff net, upper hemisphere. Density isolines: 2–7–11–18%. Asterisks indicate poles of bedding surfaces in horizons containing slump folds.

the south–southeast. Our data are in a good agreement with the data of Markevich (1970) obtained during the studies of turbidites lying at the southern part of the Sikhote–Alin Range. Markevich (1970) has studied the flute-casts in the turbidites and determined removal of detrital material in a northwest direction. The major clastic material provenance was the volcanic island arc whose basement was formed by a fragment of sialic continental crust (including the Jurassic to Early Cretaceous accretionary prism) displaced oceanward along a fault of the Tan-Lu Fault system. To supply such a great amount of clastic material, this crustal fragment had to be sizeable. Its surface, at least partially, must have been situated above sea level, as evidenced by the presence of the abundant land vegetation remains in terrigenous rocks.

The formation of the coeval terrigenous complexes of the Zhuravlevka terrane that lies west of the Kema terrane occurred in a different depositional environment within a marginal pull-apart basin (Golozoubov & Khanchuk 1995; Golozoubov 2006). The co-existence of two quite different terranes within the Sikhote–Alin region, supposed to be a secondary phenomenon, resulted from a large-scale sinistral strike-slip motion along the Tan-Lu Fault system. To restore the original positions of these paleobasins, paleogeodynamic reconstructions should be done.

GEODYNAMIC RECONSTRUCTIONS

We made an attempt to reconstruct the original position of the island-arc system using the data on the spatial distribution of the pre-Albian floras. According to Kimura (2000), there are three types of flora corresponding to the Early Cretaceous climatic zones within the eastern margin of Asia: (i) Tetori type (cold-resisting); (ii) Ryoseki type (tropical and subtropical); and (iii) mixed flora. Within the continental margin of Asia, the boundaries of climatic zones are sub-latitudinal. Along the continent–ocean border, the floral zonality is broken. For example, in the Outer Zone of Japan, the Ryoseki flora complex has been markedly displaced northward to the northern extremity of Honshu Island (no less than 15° in latitude relative

to the northern border of such flora distribution in the continent). In this area, Ryoseki flora gets in touch with Tetori type flora of the Inner Zone of Japan and the mixed flora is lacking (Kimura 1987, 2000). Farther west, within the Yamato Rise, as well as in the Early Cretaceous coal-bearing basins of the South Sikhote–Alin and the Berriasian–Valanginian turbidites of the Taukha terrane, Ryoseki flora is again recorded (Markevich 1995; Golozoubov *et al.* 1999), further complicating the general pattern of flora distribution. Markevich (1995) has analyzed palynoflora assemblages from the Aptian sandstones of the lower Kemsкая sub-formation (Malinovsky *et al.* 2002). It has been

found that the examined palynoflora spectrum is similar to those of Ryoseki flora complex (Kimura 2000). Both palynoflora assemblages are characterized by the dominance of Gleicheniaceae, Cyatheaceae and Dicksoniaceae flora; as to Gymnosperms, Taxodiales are predominant (Malinovsky *et al.* 2002). The northern border of such flora distribution on the continent was situated at approximately latitude 30° N, i.e. the Kema Basin was originally located at this latitude or even in more southern latitudes (Golozoubov *et al.* 1999; Kimura 2000).

The study area reconstruction compiled from the above data (Fig. 12) suggests that the Moneron–

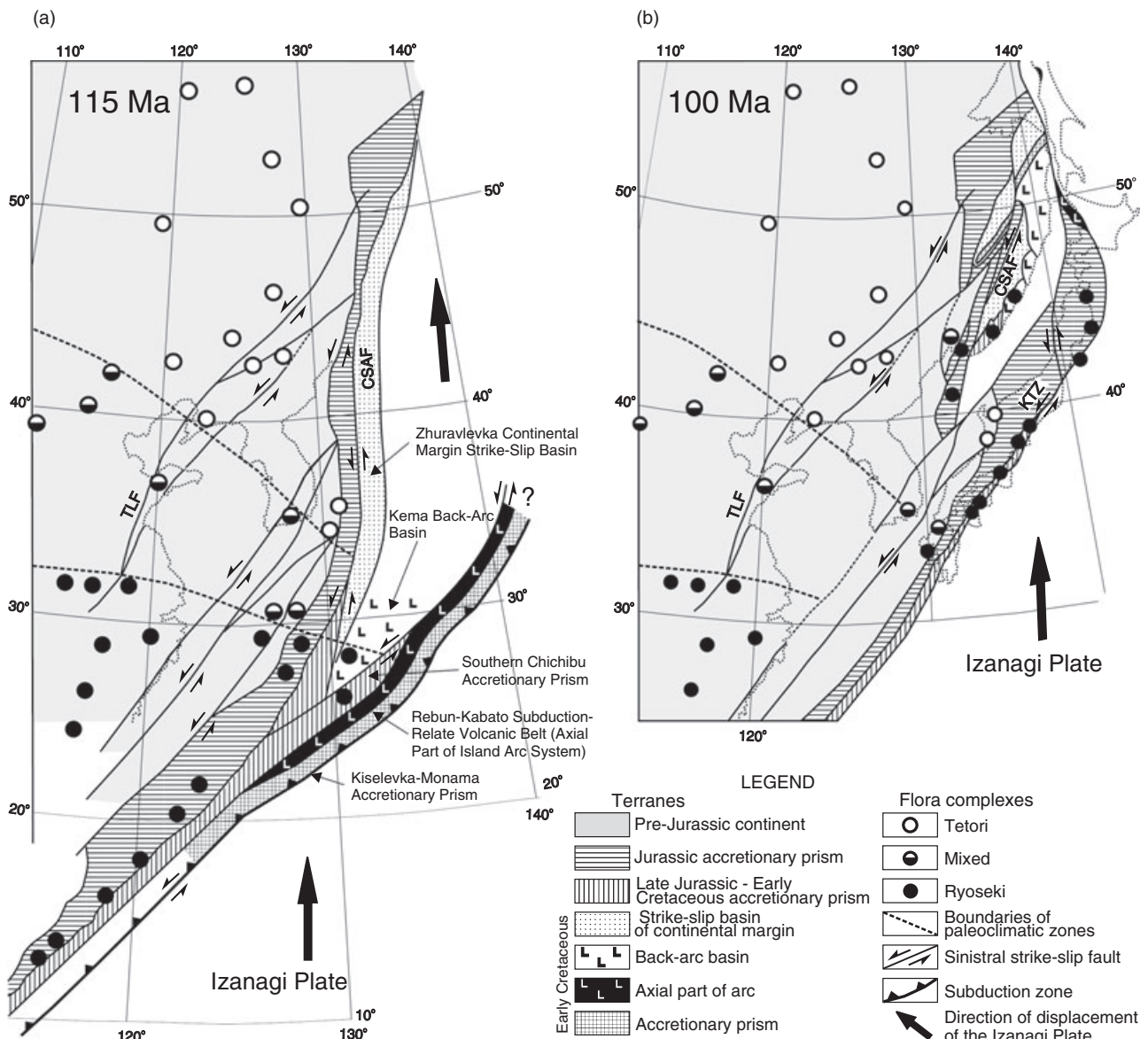


Fig. 12 Geodynamic reconstructions of the East Asian continental margin for (a) 115 Ma (before major motion along the Tan-Lu fault zone) and (b) 100 Ma (before the opening of Japan Sea). TLF, Tan-Lu Fault; CSAF, Central Sikhote–Alin Fault; KTZ, Kurosegawa Tectonic Zone.

Samarga island-arc system, which we assume to have been located nearby, was situated at the site of a change of strike of the continent's edge. The south China segment of the continental margin, lying south of this bend, trended northeast (~45°), while the northern part of the continent-ocean border extended submeridionally. In conditions of northward movement of the adjacent oceanic Izanagi Plate, it is possible to assume oblique subduction along the east China continental margin. However, to the north of the bend, there was a site of transform faulting where the Zhuravlevka terrane turbidites could be accumulated. Just around the bend in the continental plate strike, the fragment of this plate may have been extruded toward the ocean and later became basement for the Moneron–Samarga island-arc system. The axial part of this system was a belt of the calc-alkaline volcanics of Rebun–Kabato, and the arc-related accretionary process forms the Kiselevka–Manoma terrane of North Sikhote–Alin (Golozoubov 2006). The present location of this terrane in the rear of the Kema terrane seems to be related to later synaccretionary deformations. The Kiselevka–Manoma terrane forms a steep-dipping core of the megafold whose formation was related to the Albian sinistral strike-slip motion along the Tan-Lu Fault system; in particular, it was related to pulling out in the northeastern direction the Early Paleozoic Alchan Bulge (Khanchuk *et al.* 2004; Golozoubov 2006). Displacements of the Kiselevka–Manoma terrane towards the northeast are quite substantial (>2500 km); however, taking into account very high rates of oceanic Izanagi Plate movement (>20 cm per year) in the north-northeastern direction relative to relatively low-mobility Eurasia during the Aptian–Albian (Engebretson *et al.* 1985), such displacements are seemingly probable.

According to this reconstruction (Fig. 12), the Kema terrane was located in the immediate proximity of the displaced fragment of Late Jurassic Accretionary Belt and was replaced laterally with the Zhuravlevka turbidite basin.

Thus, in the Barremian–Albian time, the island-arc system consisting of the back-arc basin (Kema terrane), axial part of the arc (Kamyshovy and Rebun–Kabato terranes), and accretionary prism (Kiselevka–Manoma terrane) has been in existence along the East Asia margin, i.e. further south than 30°N. The formation of the present structure of the study margin terminated mainly at the end of the Albian and beginning of the Cenomanian before the Late Cretaceous suprasubduction volcanic belt (the East Sikhote–Alin volcanic belt) began to form.

ACKNOWLEDGEMENTS

The authors thank Professor Pavel Markevich for good advice and critical comments on the manuscript; these helped significantly in improving the paper. Thanks to V. Markevich, Institute of Biology and Soil Science, FEB RAS, Vladivostok, for determination of age of palynoflora from sedimentary rocks. This study was supported by the Russian Foundation for Basic Research (Project nos. 01-05-64602 and 06-05-96081).

REFERENCES

- ARAI S. 1992. Chemistry of chromian spinel in volcanic rocks as a potential guide to magma chemistry. *Mineralogical Magazine* **56**, 173–84.
- BHATIA M. R. 1983. Plate tectonics and geochemical composition of sandstones. *Journal of Geology* **91**, 611–27.
- DICKINSON W. R., BEARD L. S., BRAKENRIDGE G. R. *et al.* 1983. Provenance of North American Phanerozoic sandstones in relation to tectonic setting. *Geological Society of America* **94**, 222–35.
- DICKINSON W. R. & SUCZEK C. A. 1979. Plate tectonics and sandstone composition. *American Association of Petroleum Geologists Bulletin* **63**, 2164–82.
- ENGBRETSON D. C., COX A. & GORDON R. G. 1985. Relative motions between oceanic and continental plates in the northern Pacific basin. *Geological Society of America, Special Paper* **206**, 1–59.
- GOLOZOUBOV V. V. 2006. *Tectonics of the Jurassic and Lower Cretaceous Complexes of the North-Western Framing of the Pacific Ocean*. Dalnauka, Vladivostok (in Russian).
- GOLOZOUBOV V. V. & KHANCHUK A. I. 1995. Taukha and Zhuravlevka terranes of South Sikhote–Alin – fragments of the Early Cretaceous margin of Asia. *Geology of the Pacific Ocean* **12**, 203–20.
- GOLOZOUBOV V. V., MARKEVICH V. S. & BUGDAEVA E. V. 1999. Early Cretaceous changes of vegetation and environment in East Asia. *Palaeogeography, Palaeoclimatology, Palaeoecology* **153**, 139–46.
- ICHIKAWA K. 1990. Pre-cretaceous terranes of Japan. In Ichikawa K., Mizutani S. & Hara I. *et al.* (eds). *Pre-Cretaceous Terranes of Japan, Pub. of IGCP Project No 224, Pre-Cretaceous Evolution of Eastern Asia*, pp. 1–11. Nippon Insatsu Shuppan, Osaka.
- IKEDA I. & KOMATSU M. 1986. Early Cretaceous volcanic rocks of Rebun Island, North Hokkaido, Japan. *Monograph of the Association for the Geological Collaboration in Japan* **31**, 51–62 (in Japanese with English abstract).
- KHANCHUK A. I., GOLOZOUBOV V. V., SIMANENKO V. P. & MALINOVSKY A. I. 2004. Giant folds with steeply dipping hinges in structures of orogenic belts:

- Evidence from Sikhote Alin. *Doklady Earth Sciences* **395**, 165–9.
- KHANCHUK A. I., RATKIN V. V., RYAZANTSEVA M. D., GOLOZOUBOV V. V. & GONOKHOVA N. G. 1995. *Geology and Mineral Deposits of Primorsky Krai (Territory)*. Dalnauka, Vladivostok (in Russian).
- KIMURA G., SAKAKIBARA M. & OKAMURA M. 1994. Plumes in central Panthalassa? Deductions from accreted oceanic fragments in Japan. *Tectonics* **13**, 905–16.
- KIMURA T. 1987. Recent knowledge of Jurassic and Early Cretaceous floras in Japan and phytogeography of this time in East Asia. *Bulletin of the Tokyo University*, Sect. IV **39**, 87–115.
- KIMURA T. 2000. Early Cretaceous climatic provinces in Japan and adjacent regions on the basis of fossil land plants. In Okada H. & Mateer N. J. (eds). *Cretaceous Environments of Asia*, pp. 155–61. Elsevier, Amsterdam.
- KUMON F., KIMINAMI K., ADACHI M. *et al.* 1992. Modal compositions of representative sandstones from the Japanese Islands and their tectonic implications. In Kumon F., Kiminami K., Musashino M., Okada H. & Shiki T. (eds). *Composition and origin of clastic rocks from mobile belts. The Memoirs of the Geological Society of Japan* **38**, 385–401 (in Japanese with English abstract).
- LETERRIER J., MAURY R. C. & THONON P. 1982. Clinopyroxene composition as a method of identification of the magmatic affinities of paleo-volcanic series. *Earth and Planetary Science Letters* **59**, 139–54.
- MALINOVSKY A. I., PHILIPPOV A. N., GOLOZOUBOV V. V., SIMANENKO V. P. & MARKEVICH V. S. 2002. Early Cretaceous deposits of the Kema River basin (the East Sikhote-Alin region): Sedimentary infilling of back-arc basin. *Tikhookeanskaya Geologiya* **21**, 52–66 (in Russian).
- MARKEVICH P. V. 1970. *Flysch Formation of the Eastern Sikhote-Alin*. Dalnauka, Vladivostok (in Russian).
- MARKEVICH P. V., KONOVALOV V. P., MALINOVSKY A. I. & PHILIPPOV A. N. 2000. *Early Cretaceous Deposits in the Sikhote-Alin Region*. Dalnauka, Vladivostok (in Russian).
- MARKEVICH P. V., PHILIPPOV A. N., MALINOVSKY A. I., ZYABREV S. V., NECHAEV V. P. & VYSOTSKIY S. V. 1997. *Cretaceous Volcano-Sedimentary Deposits of Lower Priamurie. (Structure, Composition and Environments of Deposition)*. Dalnauka, Vladivostok (in Russian).
- MARKEVICH V. S. 1995. *The Cretaceous Palynoflora of the North of East Asia*. Dalnauka, Vladivostok (in Russian).
- MAYNARD J. B., VALLONI R. & YU H. S. 1982. Composition of modern deep-sea sands from arc-related basins. In Leggett J. K. (ed.). *Trench-forearc Geology: Geological Society of London Special Publication*, Vol. 10, pp. 551–61. Blackwell Scientific Publications, Oxford.
- MIRONOV Yu. V. 1990. Correlation between titanium and potassium in basalts as indicator of tectonic environment. *Doklady AN SSSR* **314**, 1484–7 (in Russian).
- NAGATA M., KITO N. & NIIDA K. 1986. The Kumaneshiri Group in the Kabato Mountains: The age and nature as an Early Cretaceous volcanic arc. *Monograph of the Association for the Geological Collaboration in Japan* **31**, 63–79 (in Japanese with English abstract).
- NECHAEV V. P. & ISPHORDING W. C. 1993. Heavy-mineral assemblages of continental margins as indicators of plate-tectonic environments. *Journal of Sedimentary Petrology* **63**, 1110–17.
- NECHAEV V. P., MARKEVICH P. V., MALINOVSKY A. I., PHILIPPOV A. N. & VYSOTSKY S. V. 1996. Tectonic settings of deposition of the Cretaceous sediments from the Lower Amur region, Russian Far East. *Journal of the Sedimentological Society of Japan* **43**, 69–81.
- NISBET E. G. & PEARCE J. A. 1977. Clinopyroxene composition in mafic lavas from different tectonic settings. *Contributions to Mineralogy and Petrology* **63**, 149–60.
- PECCERILLO R. & TAYLOR S. R. 1976. Geochemistry of Eocene calc-alkaline volcanic rocks from the Kastamonu area, northern Turkey. *Contributions to Mineralogy and Petrology* **58**, 63–81.
- PETTIJOHN F. J. 1975. *Sedimentary Rocks*. Harper & Row, New York.
- PISKUNOV B. N. & KHVEDCHUK I. M. 1976. New data on composition and age of Moneron Island deposits (the northern part of the sea of Japan). *Doklady AN SSSR* **226**, 647–50 (in Russian).
- RASSKAZOV S. V., SARANINA E. V., MARTYNOV Yu. A. *et al.* 2003. Using Evolution of Late Cenozoic magmatism at the active continental margin of Southern Primorye. *Tikhookeanskaya Geologiya* **22**, 92–109 (in Russian).
- ROLLINSON H. R. 1994. *Using Geochemical Data: Evaluation, Presentation, Interpretation*. Longman Group UK Ltd., London.
- SHERVAIS J. W. 1982. Ti-V plots and the petrogenesis of modern and ophiolitic lavas. *Earth and Planetary Science Letters* **59**, 101–18.
- SIMANENKO V. P. 1986. Late Mesozoic volcanic arcs of the East Sikhote-Alin and of Sakhalin Island. *Tikhookeanskaya Geologiya* **1**, 7–13 (in Russian).
- SIMANENKO V. P. 1991. Basalt-andesite assemblages of the Paleozoic and Mesozoic island arcs. In Scheglov A. D. & Zimin S. S. (eds). *The Pacific Margin of Asia. Magmatism*, pp. 58–72. Nauka, Moscow (in Russian).
- SIMANENKO V. P., MALINOVSKY A. I. & GOLOZOUBOV V. V. 2004. Early Cretaceous basalts of the Kema terrane, a fragment of the Moneron-Samarga island arc system. *Tikhookeanskaya Geologiya* **23**, 30–51 (in Russian).
- SUN S. S. & MCDONOUGH W. F. 1989. Chemical and isotopic systematics of oceanic basalts: Implications

- for mantle composition and processes. In Saunders A. D. & Norry M. J. (eds). *Magmatism in the Oceanic Basins*. Geological Society of London, Special Publication 42, pp. 313–45.
- UTKIN V. P. 1980. *Strike-slip Dislocations and Methods for Their Study*. Nauka, Moscow (in Russian).
- WALKER R. G. 1978. Deep-water sandstone facies and ancient submarine fans: Model for exploration for stratigraphic traps. *American Association of Petroleum Geologists Bulletin* **62**, 932–66.
- WOOD D. A. 1980. The application of a Th-Hf-Ta diagram to problems of tectonomagmatic classification and to establishing the nature of crustal contamination of basaltic lavas of the British Tertiary volcanic province. *Earth and Planetary Science Letters* **50**, 11–30.